Above-bandgap Photo-Induced Stabilization of Engineered Ferroelectric Domains

Haoxin Mai[1], Teng Lu[1], Qian Li[2,*], Zhifu Liu[3], Yongxiang Li[3], Felipe Kremer[4], Li Li[5], Ray L. Withers[1], Haidan Wen[2]and Yun Liu[1,*]

[1]Research School of Chemistry, The Australian National University, ACT 2601, Australia

[2]Advanced Photon Source, Argonne National Laboratory, Argonne, Illinois 60439, USA

[3]The Key Lab of Inorganic Functional Materials and Devices, Shanghai Institute of Ceramics, Chinese Academy of Sciences, Shanghai 200050, P. R. China

[4]Centre for Advanced Microscopy, Australian National University, 131 Garran Road, Acton 2601, Australia

[5]Australian National Fabrication Facility, Department of Electronic Materials Engineering, Research School of Physics and Engineering, The Australian National University, Canberra, ACT 2601, Australia

KEYWORDS: Above-bandgap illumination, ferroelectrics, domain, relaxation time, PFM, KPFM, Surface

ABSTRACT: The effect of above-bandgap photons on the domains of $BiFeO_3$ thin film was investigated via piezoresponse force microscopy (PFM) and Kelvin probe force microscopy (KPFM). It is found that under the above bandgap illumination, the relaxation time of the polarization state was significantly extended while the effective polarizing voltage for the pristine domains was reduced. We propose that this photo-induced domain stabilization can be attributed to the interaction between photogenerated surface charges and domains. Importantly, similar phenomenon is observed in other ferroelectric materials with an internal electric field once they are illuminated by above-bandgap light, indicating that this photo-induced stabilization is potentially universal rather than specific to $BiFeO_3$. Thus, this study will not only contribute to the knowledge of photovoltaic phenomena but also provide a new route to promote the stability of photovoltaic and ferroelectric materials.

1. INTRODUCTION

The effects of above-bandgap photons on ferroelectric (FE) semiconductors have attracted intense interest due to the wide applications in photovoltaic (PV) and photomemory devices[1-16]. One of the key factors to achieve these devices is to prevent the recombination of the electrons and holes that are generated by the above-bandgap illumination, and a stable internal field is thus required to separate the photo-generated carriers efficiently[1]. Current studies show that the internal fields of FE materials are derived from the FE domains (polarization and domain walls), therefore, how to maintain the stability of the FE domains, especially under the above-bandgap illumination, is of great importance[1-8].

Over the past twenty years, the influence of above-bandgap photons on FE domains has been investigated but always been a debated topic[17-27]. There were reports about the enhancement in the coercive fields (E_c) of FE crystals under above-bandgap laser illumination[17], where a photo-generated space charge mechanism was assigned. Nevertheless, contradicting observations, e.g. that above-bandgap light reduces the coercive fields, were also reported. These observations were attributed to the screening effect of the photo-generated electronic carriers on pinning defects, which promoted the propagation of smoother domain walls[18-19]. Many of these mechanisms, however, have been hypothetical and lack of support from direct observations of the interaction between photo-generated charge and FE polarization. More recently, Kelvin probe force microscopy (KPFM) has been introduced to illustrate the local interactions between FE domains and excitons via observing the evolution of surface potential (SP) induced by above-bandgap photons[20-25]. It is demonstrated that the dynamics of the photo-induced charges is strongly affected by the direction of the polarization contributed from both bulk ferroelectric photovoltaic (FE PV) effect and the number-dependent domain walls[22]. The photo-induced recovery of the SP contrast between the adjacent oppositely polarized domains has also been discovered[23]. As there is strong coupling between FE polarization and surface charges[25-27], it can be inferred that the stability of the FE domains could be affected by the photo-induced surface charges. The influence of the photo-excited surface charges on FE domains is indeed observed by Wang et al., who attributed this photo-induced stability on FE domains to the effects of surface defects[26]. The understanding of direct interactions between above-bandgap photons and FE domains, however, is still limited.

These studies therefore bring forth the question of the nature of the interaction between above-bandgap photons and FE domains: what is the direct effect of the photo-induced surface charges on the FE domains, and is the photo-induced stabilization on FE domains intrinsic property? Furthermore, if the photo-induced stabilization of FE domains is an intrinsic property, it is expected that materials showing FE domains only under high electric fields, such as anti-ferroelectric materials, would also maintain the FE domains stability under above-bandgap illumination, and thus could be considered as the candidates of photovoltaics[28]. Hence, in present work, we demonstrate direct observations of the photo-induced FE domain stabilization using KPFM and local piezoresponse hysteresis loop measurements. Among FE materials, $BiFeO_3$ (BFO) is exceptional due to its large polarization and narrow

electronic bandgap (2.2 – 2.8 eV), and thus shows promising FEPV effects[29-33]. Although it is still far away from constructing practical BFO-based PV devices, a recent attempt of combining BFO with TiO_2 and NiO as a "dye-sensitized solar cells like" structure is considered to be a highly tunable and stable PV device with good power conversion efficiency, indicating that BFO indeed can be recognized as a potential FE PV candidate.[33] Therefore, in this report, we choose BFO thin films as a model system to illustrate the photo-induced FE domain stabilization effect. We further reveal that this effect stems from the interaction of photogenerated charges and FE polarization. This study thus provides significant guidelines for the development of high efficient photovoltaic and ferroelectric materials with stable performance.

2. EXPERIMENTAL SECTION

2.1 BFO/$LaNiO_3$/Y_2O_3/Si structure fabrication. In this study, the BFO/$LaNiO_3$/Y_2O_3/Si structure was fabricated using the pulsed laser deposition (PLD) technique. An excimer laser (KrF, λ = 248 nm) was used to ablate Y_2O_3, $LaNiO_3$ (LNO), and BFOtargets.The laser repetition rate was set at 5 Hz, and the target-to-substrate distance was kept as 5 cm.First, a 50 nm Y_2O_3 layer was deposited on a (001) silicon wafer[34], using 1.5 J/cm^2 laser power density and 30 min deposition time. The oxygen pressure used was 1×10^{-5}torr, and the substrate temperature was 750 °C. Second, a20 nm layer of LNO was deposited on the as-prepared Y_2O_3 layer. The laser power density was 2.5 J/cm^2 and the deposition time was 15 min. The oxygen pressure was 5×10^{-2}torr, and the substrate temperature was 750 °C. Third, 75 nm BFO layer was deposited on the LNO/Y_2O_3/Si layer. The laser power density was 2.5 J/cm^2 and the deposition time was 60 min. The oxygen pressure was 5×10^{-2}torr, and the substrate temperature was 750 °C. Finally, the as-deposited thin films were annealed at 750 °C for 30 min under 400 Torr O_2.

2.2 Characterization. The crystallinity of the BFO thinfilmswas investigatedwith X-ray diffraction (XRD) and micro-diffraction imaging, both using 11 keV X-ray beamsat Sector 7-ID-C, Advanced Photon Source, Argonne. The standard thin-film XRD was performed on a Huber six-circle diffractometer coupled with a Pilatus 100K area detector. For X-ray imaging, an X-ray beam with a FWHM (full width at half maximum) size of ~350 nm was obtained using zone-plate focusing optics, and was raster-scanned over the BFO thin films which were aligned according to the 110_C specular diffraction conditions. The diffracted X-ray beam was detected using a Pilatus 100K area detector, on which a large region-of-interest was defined to record the total Bragg peak intensities at each scan point. UV-visible absorption spectra were measured on a UV-Vis-NIR Spectrophotometer using the diffuse reflection method (Varian Cary 5E). High-resolution transmission electron microscopy(HRTEM) and selected area diffraction (SAD) images were obtained on JEOL-2100F. Piezoresponse force microscopy (PFM) characterizations were performed under ambient conditions on a commercial AFM system (Cypher, Asylum Research), which has integrated signal generator and lock-in amplifier modules. Olympus AC240TM conductive silicon probes (Tip coating: 5 nm/20 nm Ti/Pt; force constant: calibrated 1.8 N/m) were used. The imaging contact set-points used were around 100 nN. For PFM domain imaging, we used off contact-resonance ac probing signals (typically 300 kHz, amplitude VAC = 300 mV) to excite surface oscillations. KPFM was performed in a dual-pass mode with a tip lift height of ~ 50 nm. For in-situ photo excitation measurements, the sample regions underneath the tip were illuminated by a continuous-wave laser of 458 nm wavelength (power: 0–300mW, Spectra-Physics) or another continuous-wave laser of 351-364 nm wavelength (power: 0–50mW, Coherent). Both lasers were introduced to the AFM with an optical fibre, emitting onto a circular spot with a diameter of ~0.74 mm(the former) and ~0.88 mm(the latter).The laser incidence angle with respect to the sample surface is ~10˚ to the substrate. To prevent blocking of the laser beam by the tip cantilever, the scan directions, both X and Y, were kept reverse to the incident direction (Scheme 1).

Scheme 1. Schematic of BFO thin films being poled or scanned under the illumination of 458 nm laser (2.71 eV).

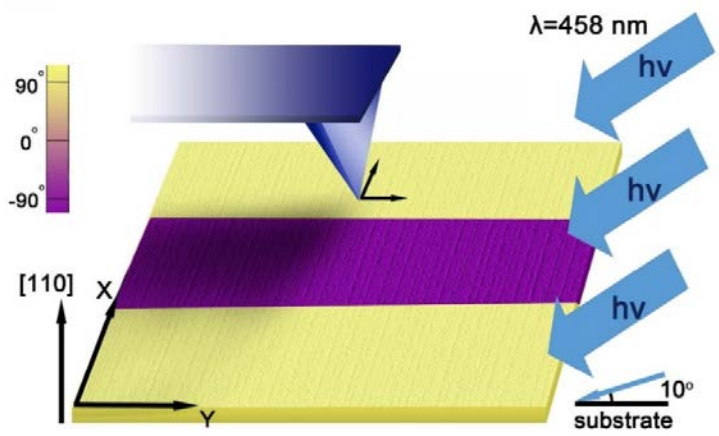

3. RESULTS AND DISCUSSION

3.1 Characterizations of BFO thin films. Figures 1a and 1b show the structurecharacterizations of the as-prepared BFO thin films. The specular XRD spectra (Figure 1a) indicate a $[110]_C$ (in the cubic phase indices) crystal orientation along the out-of-plane direction of the as-prepared films and no minor phases can be observed. The rocking-curve angular width of the specular 110_C peaks is ~1.54° (see Figure 1b), suggesting a high degree of preferred orientation. Furthermore, X-ray diffraction maps were acquired over a typical region of 20 × 20 μm^2 based on the BFO $[110]_C$. As illustrated in Figure 1b Inset and Figure S1b, these maps show small diffraction intensity variation across the region which excludes the presence of significantly misaligned grains or

secondary phases and thus attest to the relatively good crystalline quality of our BFO thin-films. Compared to the AFM topography which shows granular features in a few hundred nm size (root square roughness ~0.8 nm; see Figure 1c), the X-ray imaging shows much larger, up to several microns features presumably due to the correlated alignment of the grains. Figure 1d shows that the interfaces between BFO/LNO and LNO/Y_2O_3 are sharp and well-defined, and the thickness of Y_2O_3, LNO and BFO is approximately 50 nm, 20 nm and 75 nm, respectively. The cross-sectional HRTEM image also demonstrates the high crystalline quality of the BFO/LNO/Y_2O_3 structure (Figure S2). The $[110]_C$ preferential orientation of the BFO layer along the out-of-plane direction on the LNO/Y_2O_3 layers is confirmed with the d_{110} of the BFO layer (0.279 nm) and the SAD pattern (Figure S2). The bandgap of the sample calculated from the measured UV-vis absorption spectrum is ~2.6 eV (Figure 1e), which is in agreement with other reports[31]. A typical PFM image of the pristine thin films is shown in Figure S1c, in which no uniform domain pattern is observed.

3.2 Photo-induced stabilization on domains. Here, we explore the poling effect in a region of 1.5 μm × 1.5 μm as-prepared BFO thin film. Figure 2a illustrates the out-of-plane PFM phase images acquired at different time periods after poling, in which the bright regions correspond to the polarization directing away from the surface (c^- domain), while at the dark region the polarization directs towards the surface (c^+ domain). It is evident that strong phase contrast between c^+ domain and c^- domain formed immediately after poling (Figure 2a, top). However, such a phase contrast reduced gradually and completely disappeared after staying in dark for 6 h (Figure 2a, bottom), implying a fast relaxation of the polarization (or depolarization) in the written domains. This result is in accordance with the report of Kan et al., in which fast relaxation was observed in the small written domains when the ferroelectric crystal was thin[35-36]. Here, we define the relaxation time of domains as the time when the phase contrast between c^+ domain and c^- domain completely disappears in the PFM image.

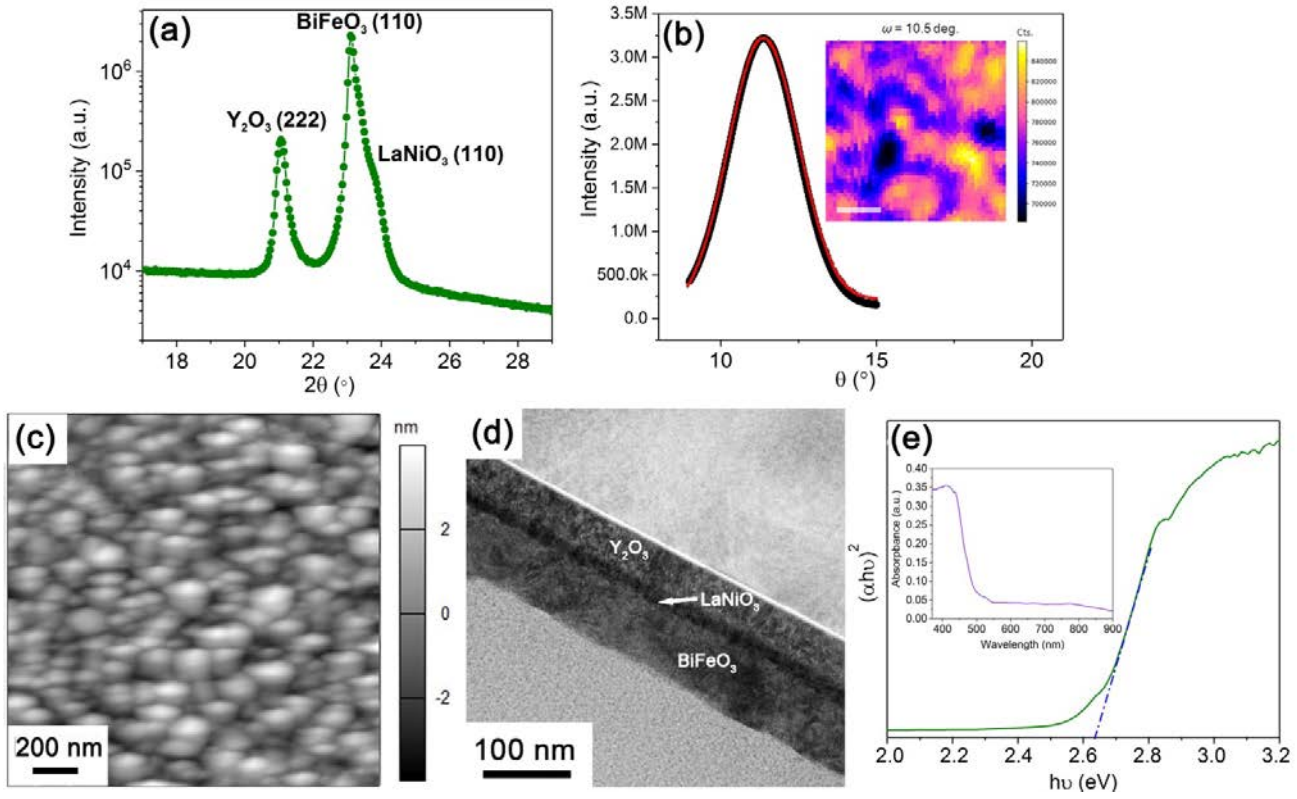

Figure 1. Characterization of as-prepared BFO thin films. (a) Specular scan XRD pattern (b) rocking curve scan around the BFO 110_C reflection along with the Gaussian peak fit (FWHM ~ 1.54°); inset is a scanning X-ray diffraction map based on the BFO 110_C reflection measured at the rocking angle ω = 10.5° (Scale bar = 5 μm). (c) AFM image of the BFO thin film in a region of 1.5 × 1.5 μm^2. (d) Cross-section TEM image of the BFO thin film. (e) Calculated band gap of the BFO thin films with the tangent of the linear part as dotted line (Inset is the raw UV–vis absorption spectrum).

When the poling is performed under 458 nm laser illumination, the time of depolarization is found to be extended remarkably. Figure 2b shows the changes of the phase contrast with time under illumination. Although the PFM image obtained immediately after the poling (Figure 2b, top) shows almost no difference with that poled in dark (Figure 2a, top), apparent phase contrast still remains after 6 h (Figure2b, bottom), and weak contrast can be observed even 24 h after poling (Figure S3a). These results evidence that the polarized region become more stable when it is poled under laser illumination. The relaxation time of polarization is estimated to be 48 h (Figure S3b), much longer than the one poled without laser illumination (6 h). As neither the applied bias nor the polarized region is different in these two measurements, the introduction of the laser during poling is the only factor that leads to the stabilization of the domains. Note that the relaxation of the written domains is mainly affected by domain wall tension and depolarization fields[36], we suggest that the above-bandgap photons affect the depolarization fields of our sample.

We also notice that phase contrast can be created by applying a lower bias under illumination than the bias applied in dark. Evident phase contrast is observed when the sample is poled with ±4 V bias under 458 nm laser illumination, though the phase differences are not 180˚ (Figure S4a). As comparison, no phase contrast will be found when this region is polarized by the same bias in dark (Figure S4b). From these results, we can conclude that the writing domain patterns would be created with lower tip-bias and have longer relaxation time under above bandgap illumination.

3.3 Surface potential in dark and under illumination. According to the previous reports, the relaxation of written domain is influenced by the depolarization field[36], which is affected by the surface charge screening[25-26]. Therefore, to further elucidate the factors of the domain stability in the as-prepared BFO thin film, KPFM is employed to examine the distribution of surface charge and the variation of SP as a function of time. Figure 3 depicts the evolution of surface potential of the BFO thin film poled in dark or under laser. In the former case, both the negative and positive charges almost distribute equally in the corresponding polarized regions soon after poling, since all of them are screening charges which are only created to compensate the polarization charge (Figure 3a, 0 min)[23]. As the time elapsed, SP reduced in both c^+ and c^- domains with the profile remaining (Figure 3a and 3b). No SP contrast is observed after 6 hours (Figure 3b, bottom). Considering that surface charges are bound by FE domains and released with the relaxation of domains, it is expected that the relaxation time of surface charges is in line with the domain relaxation (Figure 3a, bottom). The evolution of surface charges is also reflected by the time dependence of SP shown in Figures S5a – S5d. The SP decay lengths in bulk (far away from the boundaries) are estimated to be 250 - 180 min by an exponential decay function fitting, while the SP decay lengths close to the domain boundaries are 120 – 50 min, indicating that the SP decay in bulk is slower than that at boundaries when the sample is kept in dark (Figures S5a – S5d). As the relaxation of domain is consistent with the time dependent SP (Figure 2a and 3b), it is suggested that the SP decay is attributed to the diminishment of the surface screening charges. As a result, surface charges in bulk will be released once the domains are relaxed, whereas surface charges at boundaries are affected by both depolarization and recombination with the charges in the adjacent domains and thus the decay lengths are shorter. It is worth noting that the asymmetry between the SP at the c^-/c^+ and the c^+/c^- boundaries can be ascribed to the charging differences when the AFM tip move towards the c^-/c^+ boundary and away from the c^+/c^- boundary, which is in agreement with our previous work[37].

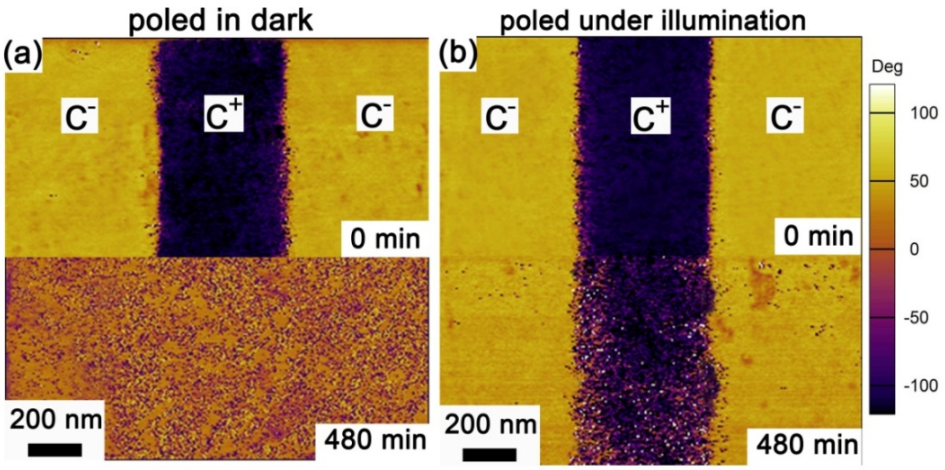

Figure 2. Photo-induced stabilization of the tip-written domains. (a) Domain patterns from a 1.5 × 1.5 μm^2 region poled with ±10 V tip bias in dark, immediately after poling (top) and after an elapsed time of 480 min (bottom). (b) Domain patterns from the same region poled with ±10 V tip bias under the illumination of a 458 nm/240 mW laser. The images were acquired in dark 0 min (top) and 480 min (bottom) after the poling.

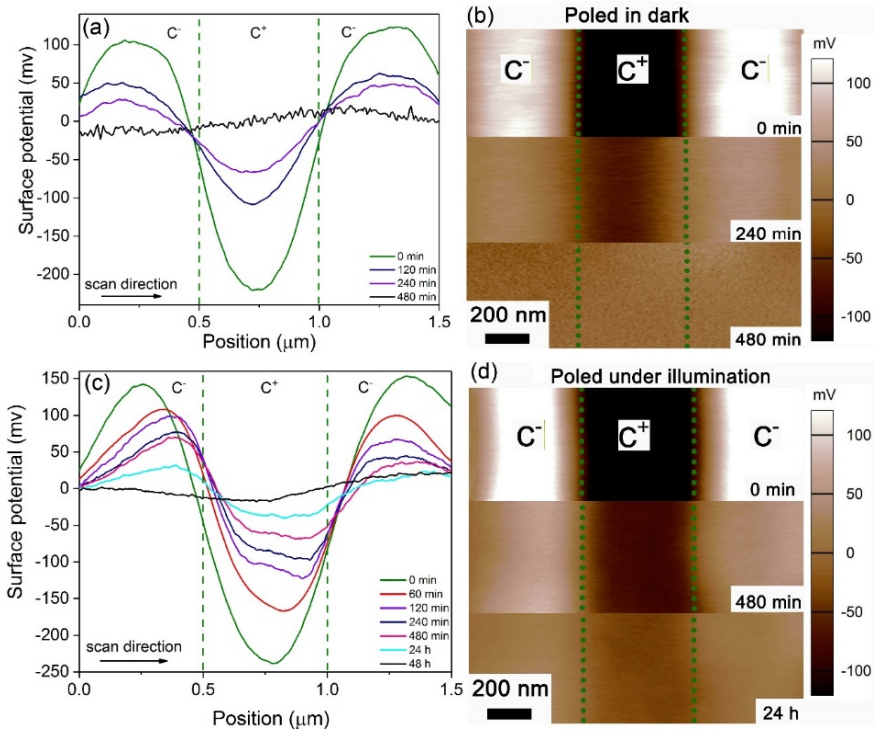

Figure 3. Decay of surface potential. (a,c) Line average profiles of the surface potential acquired in dark at different time periods after the sample region was poled in dark (a) and under illumination (c). (b, d) The corresponding KPFM images measured at a number of decay times(marked on the) for the poling in dark case (b) and poling under illumination case (d) The patterned domain boundaries are indicated with green dotted lines. The region shown here is the same as Figure 2 and the poling biases are also the same.

Scheme 2. **Mechanism of photo-induced stabilization of domains in BFO.** Schematic of the band diagrams in dark at the surface of (a) c^+ and (b) c^- domain. Schematic movement of photo-generated charges in (c) c^+ and (d) c^-domain under the illumination by a 458 nm laser. (e) A panorama sketch of the movement of photo-generated electrons under laser. E_c, E_v, and E_F denote the conduction band, valence band, and Fermi level of BFO, respectively; + and − denote the surface screening charges, while ⊕ and ⊖ denote the photo-generated holes and electrons; the dark blue arrows denote the direction of the movement of electrons; the regions in red and blue stand for the bands being bent upwards and downwards, respectively

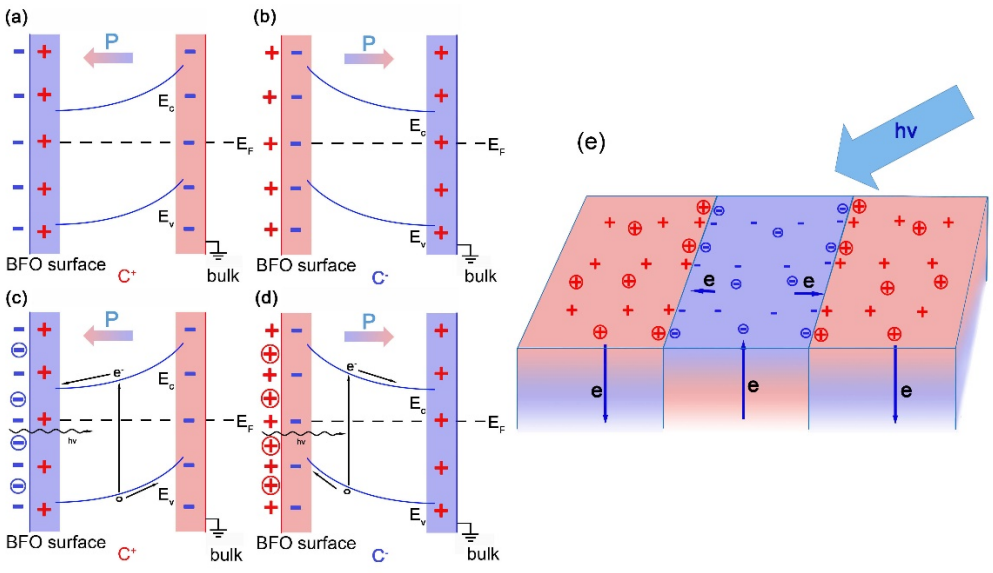

In the case of laser-assisted poling, the time dependent SP shows a few differences compared with the former case (Figures 3c and 3d). Firstly, the maximum absolute value of SP soon after poling in both c^+ and c^- domains are higher, indicating that there are more surface charges generated under illumination. Secondly, the SP contrasts remain much longer. Slight SP contrasts can still be observed in

KPFM image even after more than 24 h (Figure 3d), and we estimate that the surface charges are completely released by 48 h (Figures 3c and S6f). Thirdly, the maximum SP migrates towards the boundaries with time in c^- domains, while the SP lines show small concaves near the boundaries in c^+ domains after 2 h (Figure 3c), implying that part of the surface charges are moving from the domain centre to boundaries. The time dependence of SP also shows that while the SP decays in bulk still follow the exponential decay function, most of the points close to boundaries exhibit much slower SP decay and can no longer be fitted by the exponential decay function, especially in the first few hours (Figures S6a – S6d). As all these differences are only observed when the sample is poled under illumination, it can be proposed that these special SP decay behaviors are induced by the above-bandgap photons which generate extra surface charges that will have different behaviors on the surface of polarized regions. Again, it must be pointed out that the relaxation time of domains is also elongated to the similar extent of the SP decay (Figures 2b and 3d), and thus it is convinced that surface charges play a crucial role in the domain relaxation process.

3.4 Mechanism of photo-induced stabilization of domains. In order to explore other possible factors that may affect the domain stability, the power dependent relaxation time was firstly measured. Figure S7 shows that the relaxation time of the polarization increases with enhancing the laser power from 27mW to 240 mW and then saturates at about 48 h after the power is over 240 mW. These results indicate that the extension of depolarization observed above is resulted from the ferroelectric photovoltaic effect rather than thermal effects, as it is well known that coercive field decreases and domains become unstable with increasing temperature[17]. It is worthnoting that the saturation of relaxation time with power also implies that the domain relaxation is correlated with SP, as the photovoltage becomes insensitive to the power density when the illumination power is high[38-39]. The capture of surface charges by defects or grain boundaries, which are considered to provide extra stability to domains, are also taken into account. Figure S8 is the KPFM image of the sample measured in dark and under laser alternatively without poling. The SP contrast is almost identical in the entire area and only changes as a function of time sequence: a 20 mV increase of SP is found when the laser is switched on (as there is built-in field in the BFO-LNO interface which can separate the hole-electron pairs), while the SP drops back to 0 as soon as the laser is off. We repeat this alternative laser-on and off operations over 20 times, and the corresponding SP values are of good repeatability, implying that no photogenerated surface charges is trapped by defects and grain boundaries[24, 27]. In other words, defects and grain boundaries charging may not be the main reason causing the photo-induced stabilization of domains in this work.

To describe the mechanism of the photo-induced stabilization effect, the interfacial electronic band diagrams are schematically shown in Schemes 2a – 2d. When a negative bias is applied on the BFO film, a c^+ domain is generated where the band bends downwards because of the internal polarization field (Scheme 2a), and vice versa, upwards band bending occurs in the case of positive poling bias and c^- domain is formed (Scheme2b). The band bending facilitates the accumulation of electronic screening charge on the surface (Scheme 2a and 2b)[40-41]. As a result, the SP of c^+ domains and c^- domains are different (Figure 3a). This difference of surface potential (ΔSP) will be further increased when the laser is switched on, as the internal field can separate photogenerated excitons and drive the electrons to the surface in c^+ domain (Scheme 2c) or away from the surface in c^- domain (Scheme 2d), resulting in a more negative or positive surface potential respectively (Figure 3c)[22].

Scheme 2e depicts the movement of the photogenerated electrons on the surface of BFO film under laser illumination. At the regions far away from the domain boundaries, photogenerated electrons are driven by the internal fields and move towards or away from the surface according to the polarization orientation, thus the value of SP is increased. As per the previous discussion, that domain relaxation is affected by depolarization field, due to the photogenerated charges that partly screen the depolarization field, the relaxation time of domain will be increased, and the SP decay will be extended accordingly. Furthermore, we assume that these photogenerated surface charges will migrate from the domain centre to boundaries in terms of the results of time dependent SP (Figure 3c). This assumption can be confirmed via the analysis of the direction of surface electric field. By virtue of the derivation of the SP lines, we find that the direction of the surface electric field is away from domain centre in c^- domains, and towards domain centre in c^+ domains (Figure S6e). Therefore, the photogenerated surface charges in both c^- and c^+ domains would tend to move to the boundaries (see Supporting Information for more discussion). Therefore, domain boundaries would be stabilized by the aggregation of these photo-induced surface charges, and thus the SP decay will show significant differences from that in bulk.

To further verify the interaction between domains and photo-induced surface charges, we devised in-situ local PFM phase switching measurement (Figure 4). When the laser is off, the phase hysteresis created in the first poling cycle is almost overlapping with the second hysteresis. When the laser is on, however, the loops of two different poling cycles are divergent: the first positive coercive voltage is slightly lower than that in dark but the first negative coercive voltage (~-6.2 V) is much higher than the counterpart poling in dark (~-4.5 V), while both the positive (~+6.5 V) and negative (~-6.2 V) coercive voltages are similar and more intense than the values detected in dark (~+4.9 V and -4.5 V respectively). As the photogenerated surface charges would give rise to an extra voltage U_p, domains can only be established when the external voltage U_c, the intrinsic coercive voltage U_{inc}, considered as the coercive voltage in dark, and U_p will satisfies this relation:

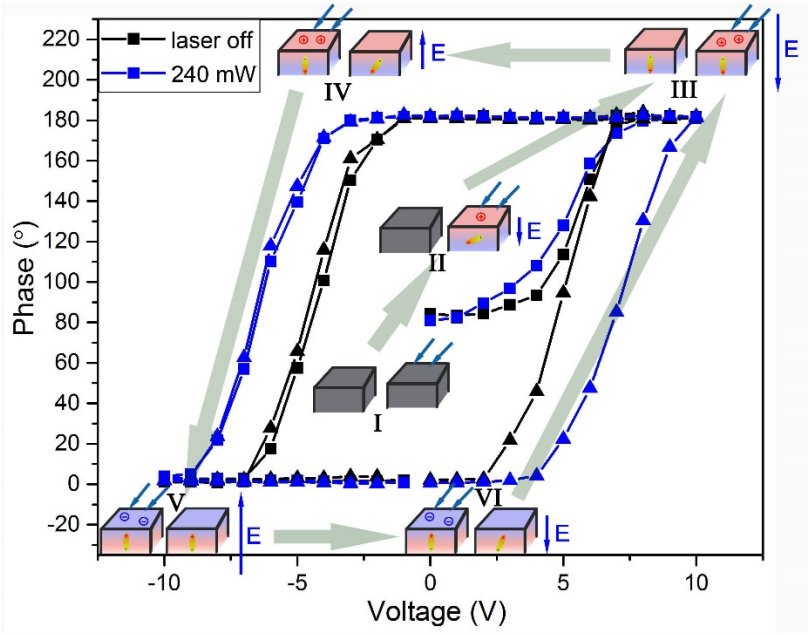

Figure 4.Effects of laser illumination on the local polarization switching behaviour. Local PFM hysteresis loops (20 spots averaged) measured at the surface of the BFO film in dark (black line) and under laser (blue line). After obtaining the loops in dark, the sample was depolarized 24 hours in dark before the switching loop measurements under the 458 nm laser. The square and triangle symbols denote the first and second cycle, respectively, of tip voltage waveforms. Insets are the schematics for the interaction between dipoles and photogenerated charges at different bias steps.

$$|U_c + U_p| > |U_{inc}| \quad (1)$$

When the sample is kept in dark, $U_p = 0$, which means that domains would be reversed as long as the external voltage is higher than the coercive voltage, and thus the hysteresis of the first and the second cycles are coincided in dark. Nevertheless, when a fresh sample is exposed under illumination, photogenerated charges can be driven to surface once there are dipoles slightly deviated to their initial states under a weak external electric field (inset of Figure 4, step II), and thus $U_p > 0$. As U_c and U_p are of the same direction, in terms of the equation (1), domains can be established even when the external voltage U_c is lower than the intrinsic coercive voltage U_{inc}. As a result, the coercive voltage indicating in the local PFM hysteresis is decreased (Figure 4), and domains with opposite orientation can then be created with the bias lower than the intrinsic coercive voltage (Figure S4a).

At the stage when the negative voltage is applied on a positive polarized sample under illumination (inset of Figure 4, step IV), the directions of U_c and U_p are different. Therefore, in order to reverse the domains, the value of the external voltage U_c must be higher than the sum of U_p and U_{inc}, indicating an enhancement of the negative coercive voltage in the local PFM hysteresis (Figure 4). Similarly, at the very beginning of the second poling cycle, domains are negatively oriented, and thus the photogenerated charges on the surface are negative, leading to the opposite direction between U_c and U_p. Hence, the positive coercive voltage of the second cycle showing in the local PFM hysteresis is much stronger than that of the first cycle and the counterpart in dark as well (Figure 4). From the results of the local PFM hysteresis and the above discussion, it can be concluded that there are interactions between domains and photogenerated surface charges, by which the polar state of the domains can be stabilized.

Similarly, the piezoresponse loops of the BFO thin film are also affected by illumination (Figure S9b). Although the height of the loops shows almost no difference when the laser is on or off, the coercive voltage of the sample kept in dark are about +4.9 V and -4.5 V, while the coercive voltage of the sample under illumination are +6.5 V and -6.1 V. In addition, we find that when the sample is under the initial stage, the positive coercive voltage of the sample under illumination is reduced to ~3.1V, about 1V lower than that of the sample in dark. All these results are in agreement with the study of the in-situ local PFM phase switching measurement, indicating that domains can be stabilized via the photo-induced surface charges.

According to this mechanism, another two results are expected. First, since the stabilization of domains is derived from the interaction between above-bandgap photons and local polarization, domains will be stabilized once they are exposed to the above-bandgap illumination, regardless of when they are polarized. In order to demonstrate this inference, the same 1.5 μm × 1.5 μm region is applied with the alternative ±10 V bias then depolarize for 2 h. The laser is kept off in this process. After that,we switch on the laser. Figure 5a and Figure S10 summarize the time dependent results of this sample. Herein, before switching on the laser, from 0 min to 120 min after poling, SP decay follows the exponential decay function in the entire polarized region (Figures 5a and S10), as it is shown in the previous results acquired in dark (Figures 3a and S5). As soon as the laser is switched on, SP contrast increases due to the generation of the photogenerated charges (Figure 5a, dark blue line), and the SP decay starts to slow down (Figure S10). As the photogenerated surface charges will also be driven by the surface electric field of which the directions are away from the domain center in c^- domains and towards the domain center in c^+ domains, it is evident that after switched on the laser, the positions of the maximum SP migrate to the boundaries in c^- domains, and there are small concaves observed at the SP lines close to the boundaries in c^+ domains (Figure 5a, from 120 min to 480 min). Such an evolution of the SP curves is identical to the variation of

the SP curves shown in Figure 3c, strongly indicating the effects of the photogenerated charges (Figures S10b – S10d). The SP contrast remains until poling after 720 min (Figures 5a and S10f), and so as the phase contrast (Figure S10h), indicating that domains are stabilized and the relaxation of domain is slower than the sample kept in dark (Figure 5a). Nevertheless, as this sample has been depolarized in dark for 2 h before the laser is switched on, the internal dipole field is attenuated and thus less photogenerated charges can be driven to the surface. As a result, the relaxation time of the polarization of this sample (12 h) is not as long as the sample poled under laser (48 h).

The second result we expect is the extra stability of domain boundaries. As the interaction between domains and photogenerated surface charges is proved, it is predictable that the more surface charges generated, the stronger interaction of the domains and surface charges can be observed, and thus the relaxation of domains will be slower. Therefore, the region close to the domain boundaries should be more stable, as photogenerated surface charges will move towards the boundaries, resulting in a slower SP decay near boundaries (Figures 3c and S6). The boundaries stability, however, is not observedin the PFM images in Figure 2. The reason we are unable to observe the extra stability of the domain boundaries is that the amount of the photogenerated charges accumulated around the domain boundaries may not be enough to bring on the stabilization that can be observed. As a result, in order to observe the extra stability of domain boundaries, it is necessary to produce more photons to pump up more photogenerated charges to the surface. There are two factors able to affect the amount of photons, the intensity of the laser illumination and the exposure time. As the laser power we used is already saturated (Figure S7), we extended the exposure time by putting the BFO thin film under laser after poling until the completion of the depolarization. More photogenerated charges would therefore be created and driven to the surface of the thin film, resulting in stronger interaction between the surface charges and the domains. Figures 5b and S11 indicate the evolution of SP, from which it can be found that the SP decay time periods are dramatically elongated, and the SP contrast can remain almost 4 days after poling, owing to more surface charges are generated. Moreover, the SP curves from 120 min to 24 h after poling show more apparent concave around the boundaries in c^+ domain, indicating that more photogenerated charges migrate to the boundaries (Figure 5b).

In accordance with the tremendous extension of the SP decay, the depolarization also becomes much slower attributed to the generation of more surface charges interacting with domains. Moreover, stabilized domain boundaries are observed in Figure 5c, wherein the boundaries remain straight and clear during the entire depolarized process, even though the phase contrast has almost disappeared completely in the other regions (Figure 5c, bottom). This excessive stability of the domain boundaries would only be observable when the photogenerated charges are adequate, therefore, neither the sample poled in dark (Figure 2a) nor the one only poled under laser but kept in dark thereafter (Figure 2b) would have enough surface charges to provide the extra stability for the domain boundaries.

3.5 Photo-induced domain stabilization in other materials.

Note that the photo-induced stabilization of domains is not relied on this particular stack of the BFO thin film structures as per the mechanism we put forward. The increases of coercive voltage of the local PFM hysteresis under illumination are also observed in the BFO thin film grown on the (100) LNO/$SrTiO_3$ substrate (Figure S12), indicating that the photo-induced stabilization of domains is an intrinsic property of the BFO thin film. In addition, the photo-induced domain stabilization described above appears not to be restricted only to BFO thin films. Similar results have been found in transparent $(Pb_{1-y}La_y)_{(1-\alpha)}(Zr_{1-x}Ti_x)_{(1-\beta)}O_3$ (7.5/65/35) (PLZT) ceramics (see Figure S13)[42], indicating that this phenomenon may be potentially universal: once a material with an internal field is exposed to above-bandgap illumination, photogenerated charges will be driven to the surface and stabilize the polar state of domains, resulting in suppressed depolarization. Furthermore, it is assumed that for some materials in which domains typically are only stable under nonzero applied electric fields (e.g. anti-ferroelectric materials), above-bandgap illumination assisted-poling may lead to a remnant stable domain state. Thus, this strategy can potentially enlarge the candidate pool of materials for applications in photovoltaic devices.

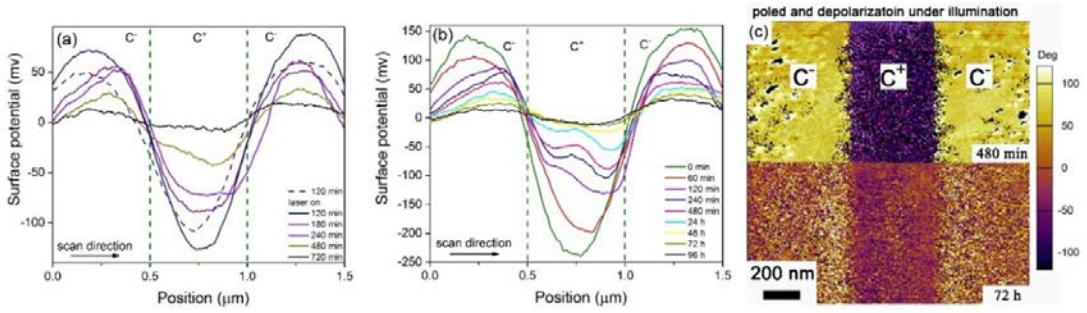

Figure 5. Effects of laser on domain stability. (a) Before switching on the laser, the sample was poled and kept in dark for 2 hours, and the line average of the surface potential is acquired from 120 min to 720 min after poling. The patterned domain boundaries are indicated with green dotted line. (b) The sample is poled under 458 nm laser then the line average of the surface potential is acquired under the same laser at different time. (c) Out of plane PFM images are obtained (top) 480 min and (bottom) 72 hours after poling under the 458 nm laser. The same biases were applied on the same region as Figure 3.

4. CONCLUSIONS

In conclusion, photo-induced stabilization of domains is discovered and studied in the BFO/LNO/Y_2O_3/Si thin film samples. The

relaxation time of the polarization of the thin film is 48 h when it is poled under the above-bandgap laser, much longer than that poled in dark (6 h), while the effective polarized voltage for the areas in the pristine state under laser is reduced to ±4 V, even lower than the coercive voltage in dark. KPFM and local PFM hysteresis are taken advantage to investigate the mechanism, and confirm that the excessive charges aggregating on the surface can stabilize the domains and result in the facilitation of polarization and extension of depolarization. In addition, we suggest that the photogenerated charges are able to shift from domain centre to domain boundaries and thus the regions around domain boundaries will show slower SP decay than the other region of the thin film, thereby providing more stability for the domain boundaries. As similar phenomenon has also been observed in the other materials (PLZT ceramic), we regard that the mechanism identified in the present work is not specific to BFO but universal, and domains will be stabilized by the excessive surface charges as long as they are exposed to the above-bandgap illumination. As it is well-known that the internal field induced by the polarization of FE semiconductors play a critical role in their PV performance, following the photon illumination method of domain engineering as we demonstrated here, it is expected that the PV outputs of FE materials will not be diminished severely due to a fast decay of the polarization and thus these results will contribute to the application of FEPV materials. Moreover, our studies can largely interpret the antiferroelectric-PV phenomena reported by Perez-Tomas et al.[28], and accordingly we would potentially obtain appreciable PV effects in antiferroelectric materials or other materials with domains that can be stabilized under above-bandgap illumination. Therefore, this study may potentially provide a new route to explore high-efficiency ferroelectric photovoltaic materials.

AUTHOR INFORMATION

Corresponding Author

*E-mail: yun.liu@anu.edu.au
*E-mail: qianli@anl.gov

Author Contributions

HM fabricated the thin films and did the KPFM and PFM characterization together with TL and YL. QL and HW did the X-ray mapping. LL prepared the cross-section sample. FK did the HRTEM and SAD. All authors contributed to discussion, result analysis and manuscript preparation.

Notes

The authors declare no competing financial interest.

ACKNOWLEDGMENT

HM, TL and YL acknowledge the support of the Australian Research Council (ARC) in the form of Discovery Projects (DP160104780). The authors acknowledge the facilities and the scientific and technical assistance of the Australian Microscopy and Microanalysis Research Facility (AMMRF) at the Centre of Advanced Microscopy, the Australian National University. The use of Advanced Photon Source was supported by the U.S. DOE, Basic Energy Science under Contract No. DE-AC02-06CH11357. QL and HW were supported by the U.S. Department of Energy, Office of Science, Materials Science and Engineering Division.

REFERENCES

1. Paillard, C.; Bai, X. F.; Infante, I. C.; Guennou, M.; Geneste, G.; Alexe, M.; Kreisel, J.; Dkhil, B., Photovoltaics with Ferroelectrics: Current Status and Beyond. *Advanced Materials* **2016,** *28* (26), 5153-5168.
2. Martin, L. W.; Rappe, A. M., Thin-film ferroelectric materials and their applications. *Nat Rev Mater* **2017,** *2* (2), 16087.
3. Choi, T.; Lee, S.; Choi, Y. J.; Kiryukhin, V.; Cheong, S. W., Switchable Ferroelectric Diode and Photovoltaic Effect in $BiFeO_3$. *Science* **2009,** *324* (5923), 63-66.
4. Yang, S. Y.; Seidel, J.; Byrnes, S. J.; Shafer, P.; Yang, C. H.; Rossell, M. D.; Yu, P.; Chu, Y. H.; Scott, J. F.; Ager, J. W.; Martin, L. W.; Ramesh, R., Above-bandgap voltages from ferroelectric photovoltaic devices. *Nat Nanotechnol* **2010,** *5* (2), 143-147.
5. Moubah, R.; Rousseau, O.; Colson, D.; Artemenko, A.; Maglione, M.; Viret, M., Photoelectric Effects in Single Domain $BiFeO_3$ Crystals. *Adv Funct Mater* **2012,** *22* (22), 4814-4818.
6. Bhatnagar, A.; Chaudhuri, A. R.; Kim, Y. H.; Hesse, D.; Alexe, M., Role of domain walls in the abnormal photovoltaic effect in $BiFeO_3$. *Nature Communications* **2013,** *4*, 2835.
7. Yang, M. M.; Bhatnagar, A.; Luo, Z. D.; Alexe, M., Enhancement of Local Photovoltaic Current at Ferroelectric Domain Walls in BiFeO3. *Sci Rep-Uk* **2017,** *7*, 43070.
8. Ahn, Y.; Park, J.; Pateras, A.; Rich, M. B.; Zhang, Q. T.; Chen, P.; Yusuf, M. H.; Wen, H. D.; Dawber, M.; Evans, P. G., Photoinduced Domain Pattern Transformation in Ferroelectric-Dielectric Superlattices. *Phys Rev Lett* **2017,** *119* (5), 057601.
9. Grinberg, I.; West, D. V.; Torres, M.; Gou, G. Y.; Stein, D. M.; Wu, L. Y.; Chen, G. N.; Gallo, E. M.; Akbashev, A. R.; Davies, P. K.; Spanier, J. E.; Rappe, A. M., Perovskite oxides for visible-light-absorbing ferroelectric and photovoltaic materials. *Nature* **2013,** *503* (7477), 509-513.
10. Zhang, J. J.; Su, X. D.; Shen, M. R.; Shen, Z. H.; Zhang, L. J.; Zhang, X. Y.; Cheng, W. X.; Cao, M. Y.; Zou, G., Enlarging photovoltaic effect: combination of classic photoelectric and ferroelectric photovoltaic effects. *Sci Rep-Uk* **2013,** *3*, 2109.
11. Nechache, R.; Harnagea, C.; Li, S.; Cardenas, L.; Huang, W.; Chakrabartty, J.; Rosei, F., Bandgap tuning of multiferroic oxide solar cells. *Nat Photonics* **2015,** *9* (1), 61-67.
12. Lu, Z. X.; Li, P. L.; Wan, J. G.; Huang, Z. F.; Tian, G.; Pan, D. F.; Fan, Z.; Gao, X. S.; Liu, J. M., Controllable Photovoltaic Effect of Microarray Derived from Epitaxial Tetragonal $BiFeO_3$ Films. *Acs Appl Mater Inter* **2017,** *9* (32), 27284-27289.
13. Lejman, M.; Vaudel, G.; Infante, I. C.; Gemeiner, P.; Gusev, V. E.; Dkhil, B.; Ruello, P., Giant ultrafast photo-induced shear strain in ferroelectric $BiFeO_3$. *Nature Communications* **2014,** *5*, 4301.
14. Biswas, P. P.; Chinthakuntla, T.; Duraisamy, D.; Venkatesan, G. N.; Venkatachalam, S.; Murugavel, P., Photovoltaic and photo-capacitance effects in ferroelectric $BiFeO_3$ thin film. *Appl Phys Lett* **2017,** *110* (19), 192906.
15. Hu, W. J.; Wang, Z. H.; Yu, W. L.; Wu, T., Optically controlled electroresistance and electrically controlled photovoltage in ferroelectric tunnel junctions. *Nature Communications* **2016,** *7*, 10808.
16. Xu, H. M.; Lin, Y. H.; Harumoto, T.; Shi, J.; Nan, C. W., Highly (001)-Textured Tetragonal $BiFeO_3$ Film and Its Photoelectrochemical Behaviors Tuned by Magnetic Field. *Acs Appl Mater Inter* **2017,** *9* (35), 30127-30132.
17. Chao, S.; Hung, C. C., Large photoinduced ferroelectric coercive field increase and photodefined domain pattern in lithium-tantalate crystal. *Appl Phys Lett* **1996,** *69* (25), 3803-3805.
18. Steigerwald, H.; von Cube, F.; Luedtke, F.; Dierolf, V.; Buse, K., Influence of heat and UV light on the coercive field of lithium niobate crystals. *Appl Phys B-Lasers O* **2010,** *101* (3), 535-539.
19. Wengler, M. C.; Fassbender, B.; Soergel, E.; Buse, K., Impact of ultraviolet light on coercive field, poling dynamics and poling quality of various lithium niobate crystals from different sources. *J Appl Phys* **2004,** *96* (5), 2816-2820.
20. Chen, X. Q.; Yamada, H.; Horiuchi, T.; Matsushige, K.; Watanabe, S.; Kawai, M.; Weiss, P. S., Surface potential of ferroelectric thin films investigated by scanning probe microscopy. *J Vac Sci Technol B* **1999,** *17* (5), 1930-1934.
21. Bednyakov, P.; Sluka, T.; Tagantsev, A.; Damjanovic, D.; Setter, N., Free-Carrier-Compensated Charged Domain Walls Produced with Super-Bandgap Illumination in Insulating Ferroelectrics. *Advanced Materials* **2016,** *28* (43), 9498-9503.
22. Yan, F.; Chen, G. N.; Lu, L.; Spanier, J. E., Dynamics of Photogenerated Surface Charge on $BiFeO_3$ Films. *Acs Nano* **2012,** *6* (3), 2353-2360.
23. Wang, L.; Jin, K. J.; Gu, J. X.; Ma, C.; He, X.; Zhang, J. D.; Wang, C.; Feng, Y.; Wan, Q.; Shi, J. A.; Gu, L.; He, M.; Lu, H. B.; Yang, G. Z., A new non-destructive readout by using photo-recovered surface potential contrast. *Sci Rep-Uk* **2014,** *4*, 6980.

24. Gu, J. X.; Jin, K. J.; Wang, L.; He, X.; Guo, H. Z.; Wang, C.; He, M.; Yang, G. Z., Long-time relaxation of photo-induced influence on $BiFeO_3$ thin films. *J Appl Phys* **2015,** *118* (20), 204103.
25. Yang, S. M.; Morozovska, A. N.; Kumar, R.; Eliseev, E. A.; Cao, Y.; Mazet, L.; Balke, N.; Jesse, S.; Vasudevan, R. K.; Dubourdieu, C.; Kalinin, S. V., Mixed electrochemical-ferroelectric states in nanoscale ferroelectrics. *Nat Phys* **2017,** *13* (8), 812-818.
26. Wang, J.; Huang, H. B.; He, W. Q.; Zhang, Q. H.; Yang, D. N.; Zhang, Y. L.; Liang, R. R.; Wang, C. S.; Ma, X. Q.; Gu, L.; Chen, L. Q.; Nan, C. W.; Zhang, J. X., Nanoscale Bandgap Tuning across an Inhomogeneous Ferroelectric Interface. *Acs Appl Mater Inter* **2017,** *9* (29), 24704-24710.
27. Bhatnagar, A.; Kim, Y. H.; Hesse, D.; Alexe, M., Persistent Photoconductivity in Strained Epitaxial $BiFeO_3$ Thin Films. *Nano Lett* **2014,** *14* (9), 5224-5228.
28. Perez-Tomas, A.; Lira-Cantu, M.; Catalan, G., Above-Bandgap Photovoltages in Antiferroelectrics. *Adv Mater* **2016,** *28* (43), 9644-9647.
29. Catalan, G.; Scott, J. F., Physics and Applications of Bismuth Ferrite. *Advanced Materials* **2009,** *21* (24), 2463-2485.
30. Zhang, Q.; Valanoor, N.; Standard, O., Epitaxial (001) $BiFeO_3$ thin-films with excellent ferroelectric properties by chemical solution deposition-the role of gelation. *J Mater Chem C* **2015,** *3* (3), 582-595.
31. Basu, S. R.; Martin, L. W.; Chu, Y. H.; Gajek, M.; Ramesh, R.; Rai, R. C.; Xu, X.; Musfeldt, J. L., Photoconductivity in $BiFeO_3$ thin films. *Appl Phys Lett* **2008,** *92* (9), 091905.
32. Wang, T.; Jin, L.; Tian, Y.; Shu, L. L.; Hu, Q. Y.; Wei, X. Y., Microstructure and ferroelectric properties of Nb_2O_5-modified $BiFeO_3$-$BaTiO_3$ lead-free ceramics for energy storage. *Mater Lett* **2014,** *137*, 79-81.
33. Wang, L.; Ma, H.; Chang, L.; Ma, C.; Yuan, G.; Wang, J.; Wu, T., Ferroelectric $BiFeO_3$ as an Oxide Dye in Highly Tunable Mesoporous All-Oxide Photovoltaic Heterojunctions. *Small* **2017,** *13* (1), 1602355.
34. Huignard, A.; Aron, A.; Aschehoug, P.; Viana, B.; Thery, J.; Laurent, A.; Perriere, J., Growth by laser ablation of Y_2O_3 and Tm : Y_2O_3 thin films for optical applications. *J Mater Chem* **2000,** *10* (2), 549-554.
35. Kan, Y.; Lu, X. M.; Bo, H. F.; Huang, F. Z.; Wu, X. B.; Zhu, J. S., Critical radii of ferroelectric domains for different decay processes in $LiNbO_3$ crystals. *Appl Phys Lett* **2007,** *91* (13), 132902.
36. Kalinin, S. V.; Morozovska, A. N.; Chen, L. Q.; Rodriguez, B. J., Local polarization dynamics in ferroelectric materials. *Rep Prog Phys* **2010,** *73* (5), 056502.
37. Lau, K.; Liu, Y.; Li, Q.; Li, Z. R.; Withers, R. L.; Xu, Z., Domain-selective photochemical reaction on oriented ferroelectric $Pb(In_{1/2}Nb_{1/2})O_3$-$Pb(Mg_{1/3}Nb_{2/3})O_3$-$PbTiO_3$ single crystals. *Appl Surf Sci* **2013,** *265*, 157-161.
38. Ji, W.; Yao, K.; Liang, Y. C., Bulk Photovoltaic Effect at Visible Wavelength in Epitaxial Ferroelectric $BiFeO_3$ Thin Films. *Advanced Materials* **2010,** *22* (15), 1763-1766.
39. Guo, R.; You, L.; Zhou, Y.; Lim, Z. S.; Zou, X.; Chen, L.; Ramesh, R.; Wang, J. L., Non-volatile memory based on the ferroelectric photovoltaic effect. *Nature Communications* **2013,** *4*, 1990.
40. Giocondi, J. L.; Rohrer, G. S., Spatial separation of photochemical oxidation and reduction reactions on the surface of ferroelectric $BaTiO_3$. *J Phys Chem B* **2001,** *105* (35), 8275-8277.
41. Tiwari, D.; Dunn, S., Photochemistry on a polarisable semi-conductor: what do we understand today? *J Mater Sci* **2009,** *44* (19), 5063-5079.
42. Withers, R. L.; Liu, Y.; Welberry, T. R., Structured diffuse scattering and the fundamental 1-d dipolar unit in PLZT $(Pb_{1-y}La_y)_{(1-\alpha)}(Zr_{1-x}Ti_x)_{(1-\beta)}O_3$ (7.5/65/35 and 7.0/60/40) transparent ferroelectric ceramics. *J Solid State Chem* **2009,** *182* (2), 348-355.

Table of Contents